Nano Research

ISSN 1998-0124 CN 11-5974/O4
https://doi.org/10.1007/s12274-023-5442-3

Research Article

Turning carbon dots into selenium bearing nanoplatforms with *in vitro* GPx-like activity and pro-oxidant activity

Laura Perez-Garrido, Mariano Ortega-Muñoz, Fernando Hernandez-Mateo, F. Javier Lopez-Jaramillo (✉), and Francisco Santoyo-Gonzalez (✉)

Department of Organic Chemistry, Biotechnology Institute, School of Sciences, Campus Fuentenueva sn, University of Granada, 18071-Granada, Spain

Received: 11 October 2022 / **Revised:** 27 December 2022 / **Accepted:** 29 December 2022

ABSTRACT

Selenium (Se) has been defined as the "Janus element", with one face showing antioxidant activity and the other pro-oxidant activity. The biological effect of Se depends on both dose and speciation. Se nanoparticles are attracting major interest, although their large-scale preparation for biomedical applications is not trivial. We hypothesize that acid anhydride-coated carbon dots (AA-CD) are an attractive platform for preparing nanoparticles containing chemically defined Se. The reaction of AA-CD with 3-selenocyanatopropan-1-amine yields carbon dots bearing selenocyanate and carboxylate groups (CD-SeCN) that allow for tuning the hydrosolubility. CD-SeCN has a Se content of 0.36 μmol per mg of nanoparticles, and they show the typical photoluminescence of carbon dots. The selenocyanate groups (SeCN) exhibited glutathione peroxidase-like activity and cytotoxicity. Data show that antioxidant behavior differs between normal and tumor cells, and the evaluation on HEK293 and A549 cells reveals that the toxicity of CD-SeCN depends on dose, time, and intracellular glutathione (GSH) content. The toxicity of CD-SeCN decreases with the time of incubation and the cell death mechanism switches from necrosis to apoptosis, indicating that CD-SeCN is neutralized. Additionally, high levels of intracellular GSH exert a protective effect. These results support a pharmacological potential in cancers with low levels of intracellular GSH. The use of AA-CD as nanoplatforms is a general strategy that paves the way for the engineering of advanced nanosystems.

KEYWORDS

selenium nanoparticles, carbon dots, glutathione peroxidase-like activity, Janus element, nanomedicine

1 Introduction

Selenium (Se) is an essential micronutrient that forms part of the active site of selenoproteins such as glutathione peroxidases (GPxs), iodothyronine deiodinase (ID), and thioredoxin reductase (TrxR) [1]. Although the evolutionary advantage of incorporating Se and its physiological role are not fully understood, it has been hypothesized that nature chose Se due to its unique ability to react reversibly with oxygen and related reactive oxygen species (ROS), conferring resistance to irreversible oxidation and inactivation [2]. Common ROS such as singlet oxygen ($^1O_2$), superoxide (O_2^{-}), hydroxyl (OH), and hydrogen peroxide (H_2O_2) are abundant in living systems and are involved in physiological processes at moderate concentrations [3]. In fact, at the physiological nanomolar range, H_2O_2 is the major signaling agent through specific protein targets. However, high levels of ROS cause oxidative stress with a destructive effect on normal cell tissues, and their role in cancer is well established [4]. Peroxiredoxins, catalase, and GPxs, regulate the level of H_2O_2 by conversion into water and oxygen [3].

Se has been designated as the "Janus element," with one face exhibiting antioxidant activity that leads to oxidative stress protection and peroxide reduction and the other exhibiting pro-oxidant activity that oxidizes free thiols and induces oxidative damage [5]. Since the rediscovery of ebselen [2-phenyl-1,2-benziselenazol-3(2H)-one] as a potent antioxidant agent with GPx-like activity [6], major efforts have been directed toward developing organoselenium compounds [5] and numerous reports have demonstrated the potential of those compounds as chemotherapeutic and/or radioprotector agents [7, 8]. The therapeutic potential of Se depends on both the dose and speciation (inorganic, organic, and nanoparticles), and the therapeutic window is narrow, with inorganic Se being more toxic than organoselenium compounds, whereas selenium nanoparticles (SeNPs) are highly biocompatible [9].

SeNPs are metallic nanoparticles of elemental Se arranged as spherical particles, nanorods, nanowires, or nanotubes [10]. SeNPs are attracting major interest in biomedicine for their application as therapeutic and theragnostic agents due to their high bioavailability and low toxicity [11–13]. Besides their antimicrobial, antidiabetic, and antiparasitic effects, and their role as biomarkers for several neurological diseases, SeNPs are promising therapeutic agents in cancer. SeNPs cause the production of ROS, cytotoxicity, and inhibition of the cell proliferation, as well as the degradation of the androgen receptors in prostate cancer and modulation of the estrogen receptor signaling in MCF-7 cells [12]. Generally, tumor cells are more susceptible to the toxic effect of Se due to the increased

Address correspondence to F. Javier Lopez-Jaramillo, fjljara@ugr.es; Francisco Santoyo-Gonzalez, fsantoyo@ugr.es

mitochondrial respiration and metabolic activities [13]. Additionally, it has been suggested that the acidic pH and the redox imbalance of the malignant cells favor the uptake of the SeNPs [13].

SeNPs can be obtained thought the physical fragmentation of Se^0. Alternatively, the reduction of the highly hazardous sodium selenite and sodium selenate or of the more benign sodium selenosulphate, selenous acid, and Se oxide is a widely used methodology [14]. Chemical reduction is the most common approach, and it uses chemical reductants (sodium borohydride, ascorbic acid, hydrazine, glucose, L-Cys...) and surfactants or growth terminating agents (polyvinylchloride, hyperbranched polysacharides...) to control the size and obtain stable colloidal solutions [10]. Both hydrothermal and microwave syntheses have been reported, but the usage of SeNPs obtained by chemical reduction in biological systems is limited by the potential toxicity of the reductants and the stabilizing agents [10]. The synthesis of SeNPs by biological methods is an alternative that relies on the ability of different organisms (bacteria and fungi) and plant extracts to reduce Se^{+4} and Se^{+6} to Se^0 and to stabilize the nanoparticles [15]. In particular, the use of plant extracts is believed to represent a superior non-hazardous approach since it eliminates the tedious procedures for maintaining the cell cultures [10].

Due to the colloidal nature of SeNPs, their large-scale preparation for biomedical applications is not trivial. In the context of nanomedicine, nanoparticles have found application [16], and carbon dots (CDs) have been recognized as therapeutic platforms [17, 18], and heteroatom doping has been proven as a suitable strategy to further improve their properties [19]. Doping of CDs with Se and codoping with Se and S have been reported, and the resulting Se-doped (SeCDs) and Se-S-codoped CDs (SeSCDs) have been shown to be non-toxic, free radical scavengers and display thioredoxin reductase activity [20–22]. However, the chemical nature of the Se in these CDs remains uncertain. X-ray photoelectron spectroscopy (XPS) spectra reveal C–Se bonds in the case of SeCDs, whereas S and Se are assumed to exist as –SH and Se–SH in the case of SeSCDs. Since the biological effects of Se depend on both dose and speciation [9], the exploration of new strategies for the synthesis of nanoparticles bearing chemically defined forms of Se is a priority to facilitate the translation of knowledge from the bench to the bedside. In this paper, we report (i) a novel strategy for the synthesis of nanosystems bearing Se based on the surface functionalization of CDs with molecules containing selenocyanate groups (SeCN), (ii) the characterization of the resulting nanosystem (CD-SeCN), and (iii) the evaluation of their biological effects on cell lines HEK293 and A549 that present different levels of glutathione (GSH).

2 Experimental

2.1 Chemicals and materials

Anhydrous citric acid, potassium selenocyanate (KSeCN), 3-bromopropan-1-amine bromohydrate, H_2O_2, thiophenol, GSH, 2-mercaptoethanol, propidium iodide (PI), fluorescein diacetate (FDA), and dialysis membranes (14,000 Da cut-off) were obtained from Sigma-Aldrich (St Louis, MO, USA). The FITC Annexin V apoptosis detection kit with PI was purchased from Immunostep (Salamanca, Spain). Commercial reagents were used as received without any further purification. Cell lines were provided by the cell bank facility at Centro de Instrumentación Científica, Universidad de Granada (CIC-UGR).

2.2 Instrumentation

XPS analyses were conducted at CIC-UGR using a Kratos Axis Ultra-DLD spectrometer (Manchester, UK), monochromatic Al Kα radiation, and XPS Peak 4.1 to process the spectra. Electron microscopy analysis was performed at CIC-UGR using a high-resolution transmission electron microscope (HRTEM) (FEI TITAN G2, Hillsboro, Oregon, USA) operated at 300 kV. Photolumiscence spectra were recorded on an F2000 fluorescence spectrophotometer (Hitachi, Tokyo, Japan). ^{77}SeNMR spectra were collected at CIC-UGR with a Bruker Nanobay Avance III HD 400 MHz equipped with a Z-gradient BBFO probe (Billerica, Massachusetts, USA). Ultraviolet–visible (UV–vis) absorption spectra were collected using a Specord 200 Plus instrument (Analytik Jena, Jena, Germany). Flow cytometry analysis was conducted at CIC-UGR using a BD FACS Canto II (Franklin Lakes, New Jersey, USA) equipped with three excitation lasers (405, 488, and 635 nm) and data were analyzed with the software DIVA6 v6.3 from DB. The X-ray diffractogram (XRD) was collected with a D8 discover equipped with a Pilatus3R 100K-A detector (Bruker), operation voltage and current of 50 kV and 1 mA respectively, and Cu Kα (λ = 1.5406 Å) sealed tube. Data were collected from 2θ 10º to 65º with a 0.02º step and 40 s of integration.

2.3 Synthesis of CD-SeCN

The syntheses of acid anhydride-coated carbon dots (AA-CD) and 3-selenocyanatopropan-1-amine hydrobromide (compound **1**) were conducted as previously reported [23]. Briefly, 10 g of citric acid was heated in an oil bath at 180 °C for 2 h in the absence of solvent to yield AA-CD. Compound **1** was obtained by the reaction of 3-bromopropan-1-amine hydrobromide (0.5 g, 2.28 mmol) with KSeCN (0.36 g, 2.5 mmol) in acetonitrile at room temperature for 14 h, and the product was isolated by filtration in good yield (90.6%).

CD-SeCN was obtained by reacting compound **1** (0.98 g, 4.0 mmol) with AA-CD (0.98 g) in the presence of triethylamine (3.6 mmol) in anhydrous methanol (10 mL) for 24 h at room temperature. The reaction was thoroughly dialyzed (molecular weight cut-off (MWCO) = 14,000 Da) against water and, after treatment with 5% HCl to protonate the carboxylic groups and reduce the hydrosolubility, extracted with ethyl acetate (3 × 20 mL), the unreacted compound **1** being eliminated in the aqueous phase. Organic phases were rotavaporated under vacuum, and the resulting solid was dissolved in a saturated solution of $NaHCO_3$ (10 mL) and extensively dialyzed (MWCO = 14,000 Da) against H_2O (6 × 5 L, 48 h). The sample was then filtered (nylon, 0.22 μm) and lyophilized to yield CD-SeCN.

2.4 Synthesis of 3,3′-diselanediylbis(propan-1-amine) (compound 2)

Se (5 mmol) was dispersed in water (10 mL) containing $NaHBH_4$ (10 mmol) under an argon atmosphere. After 20 min, an additional amount of Se (5 mmol) was added. After 10 min, 3-bromopropan-1-amine hydrobromide (10 mmol) dissolved in water (20 mL) was further added. The reaction was allowed to proceed overnight (18 h). Then, 1 M NaOH (10 mL) was added, and the product was isolated by liquid–liquid extraction with Cl_2CH_2 (3 × 50 mL) (51% overall yield).

2.5 GPx-like activity assays

Kinetic analysis of the degradation of H_2O_2 by CD-SeCN using thiophenol as a reductant was performed as described previously [24]. Briefly, different volumes of either a solution of CD-SeCN in water (3 mg/mL, 1.1 mM Se), KSeCN in water (0.32 mg/mL,

2.2 mM) or ebselen in methanol (0.38 mg/mL, 1.4 mM) were assayed in a methanol solution of H_2O_2 (2 mM) and thiophenol (1 mM) and the reaction was monitored by UV spectroscopy at 305 nm. The reduction rate was estimated as the slope of the variation of the concentration of thiophenol versus time in the linear range of the kinetics ($R^2 > 0.97$). The concentrations of thiophenol were calculated as previously described [24].

The study of catalysis using GSH as a reductant was carried out by the addition of different volumes of GSH (50 mM in water) to a buffered solution (phosphate buffered saline (PBS)) at pH 6.5 or 7 of H_2O_2 (2 mM) containing CD-SeCN (5 μg/mL, 1.8 μM of Se). The reaction was allowed to proceed at 37 °C and monitored by UV spectroscopy at 305 nm. The reduction rate was estimated as the slope of the variation of the optical density versus time in the linear range of the kinetics ($R^2 > 0.93$).

2.6 Fluorescence quantum yield (QY) determination

The fluorescence QY in water was calculated using as a standard the hydrosoluble sodium salts of the AA-CD obtained by treatment with NaOH and dialysis against water (QY = 0.04) [23], and applying [25]

$$QY = QY_{st}\left[\frac{m}{m_{st}}\right]\left[\frac{n^2}{n_{st}^2}\right] \quad (1)$$

where QY_{st} is the QY of the standard (st), m is the slope of the plot fluorescence intensity (λ_{em} 460 nm, λ_{ex} 360 nm) versus absorbance (λ 360 nm) in the range 0.015 to 0.135, and n is the refractive index (it was assumed $n = n_{st}$).

2.7 ^{77}SeNMR experiments

Compound **1**: The ^{77}SeNMR spectra were recorded from a solution of **1** in D_2O (0.15 mmol in 500 μL) after 129 scans. Then, 2-mercaptoethanol (53 μL, 0.75 mmol) was added. After shaking, new spectra were collected after 185 scans. Finally, H_2O_2 (147 μL, 1.5 mmol) was added, and 185 scans were collected.

Compound **2**: The ^{77}SeNMR spectra were recorded from a solution of the chlorhydrate of compound **2** in D_2O (0.15 mmol in 500 μL) after 119 scans. The chlorhydrate was prepared by dissolving compound **2** (20.5 mg, 0.075 mmol) in 2 M HCl (1 mL) in diethyl ether. After 30 min, the solvent was removed to yield the chlorhydrate of compound **2**.

2.8 Biological assays

Biological assays were conducted at CIC-UGR. Human embryonic kidney (HEK293; ATCC nº CRL-15739) and adenocarcinoma human alveolar basal epithelial cells (A549; ATCC nº CCL-185) were grown in Dulbecco's Modified Eagle Medium (DMEM) supplemented with 10% (v/v) fetal bovine serum (FBS), 2 mM glutamine, and 100 U/mL penicillin plus 0.1 mg/mL streptomycin. Cells were seeded in 48 well plates at a density of 1.5×10^4 cells per well and incubated at 37 °C for 24 h to reach a cell confluence of 80%–90%. Then, cells were incubated for 24 and 48 h with suitable amounts of CD-SeCN to yield the desired concentration (up to 250 μg/mL for the cytotoxicity assay and 10 μg/mL to study the cell death process). Then, cells were washed with PBS, trypsinized and pelleted. Finally, cells were resuspended in PBS to a concentration of 10^6 cells/mL and analyzed by flow cytometry. Each measurement consisted of the analysis of a population of at least 6000 events by recording forward and orthogonal light scatter, red (> 630 nm) and green (520 nm) fluorescence.

For the cytotoxicity assay, a volume of 500 μL of the cell suspension was incubated at room temperature with fluorescein diacetate (100 ng/mL, 50 μL) and propidium iodide (100 μg/mL, 50 μL) for 10 min. Fluorescein diacetate is not fluorescent, it is uptaken and retained by cells with an intact cytoplasmic membrane, and by the action of intracellular esterases, it is converted to fluorescein (green fluorescence). Propidium iodide (red fluorescence) is excluded by viable cells, but it binds to nucleic acids in dead or dying cells. Hence, viable cells fluoresce as green and non-viable cells as red.

For the study of the cell death process, the protocol included in the kit FITC annexin V apoptosis detection kit with PI (Immunostep) was followed. Cells suffering apoptosis bind annexin V and fluoresce green, at the late stage also PI, and necrotic cells bind only PI.

3 Results and discussion

We have established that the thermolysis of citric acid yields CDs decorated with acid anhydride functional groups (AA-CD) that can be functionalized with glyco-moieties and alkyl amino chains to yield glyconanoparticles [23] and amphiphilic-like CDs [26]. From this previous experience, we envision a general strategy to synthesize nanoparticles bearing chemically defined forms of Se consisting of the reaction of AA-CD with a suitable amine carrying a functional group containing selenium. As a proof of concept, we focused on 3-selenocyanatopropan-1-amine hydrobromide (compound **1**) as a suitable amine for the formation of an amide linkage by the reaction with the anhydride acid groups. The short length of the alkyl chain ensures the hydrosolubility of the resulting CD-SeCN. Additionally, some biological activity is expected since the role of the SeCN group in cancer has been known since at least 1985 [27] with a persistent interest [11]. SeCN has been reported to increase intracellular oxidative stress [28], and show GPx-like activity [29].

3.1 Synthesis and characterization of CD-SeCN

The nucleophilic displacement of the bromide atom from 3-bromopropan-1-amine hydrobromide with KSeCN allowed the straightforward preparation of compound **1** (Scheme 1) [30]. The reaction of compound **1** with freshly prepared AA-CD, obtained by solvent free thermolysis of citric acid [23] yielded the corresponding CD-SeCN (Scheme 1). These nanoparticles were purified by extensive dialysis against water and liquid–liquid extraction taking advantage of the fact that the hydrosolubility of CD-SeCN can be modulated by tuning the protonation of the carboxylic groups, CD-SeCN being isolated from the organic phase.

The characterization of CD-SeCN was performed by a variety of techniques, including XRD, XPS, HRTEM, and UV–vis spectroscopy. The X-ray diffractogram (Fig. S1 in the Electronic Supplementary Material (ESM)) shows a broad hump centered around $2\theta = 26°$, as seen in many CD XRD patterns, with some peaks at $2\theta = 23.9°$, 25.7°, and 29.5°, indicating that CD-SeCN has poor crystalline structure and a dominant amorphous character. The XPS analysis shows peaks at 54, 283, 398, 529, and 1066 eV, which are attributed to Se 3d, C 1s, N 1s, O 1s, and Na 1s, respectively (Fig. 1). The atomic concentrations of N and Se are estimated to be 0.91% and 0.52%, respectively (Fig. 1), being the N/Se ratio, within the experimental errors, close to the expected theoretical value of 2. These findings led to an estimate of the selenium content in nanoparticles of 0.36 μmol per mg. The chemical nature of Se was further studied. The Se 3d high resolution spectrum (Fig. 2(a)) presents two signals at 62.5 and 55.2 eV that are attributed to Na 2s and Se 3d of Se^{-2} respectively. The 55.2 eV signal was fitted with two peaks at 54.5 and 55.3 eV, whose separation of 0.8 eV agrees with the Se 3d spin orbit split $3d_{5/2}$ and $3d_{3/2}$ [31]. The N 1s peak (Fig. 2(b)) is fitted with two

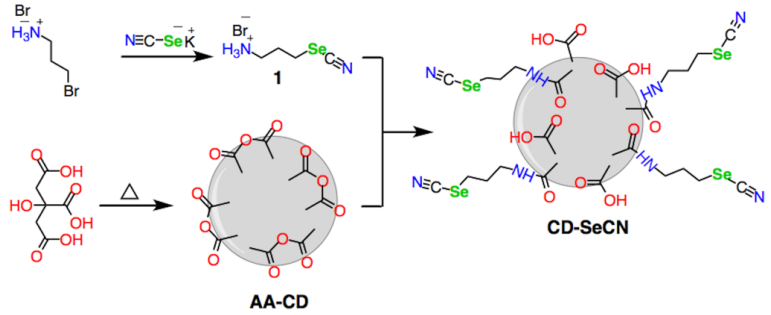

Scheme 1 Synthesis of compound **1** and nanoparticles AA-CD and CD-SeCN.

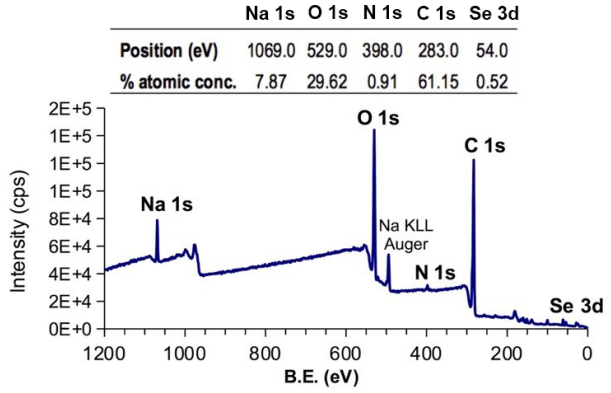

Figure 1 XPS survey spectrum of CD-SeCN showing the significant peaks and their quantification.

peaks at 398.1 and 399.7 eV that correspond to the nitrile-type and the amide-type nitrogen, respectively [32]. The C 1s peak (Fig. 2(c)) consisted of four peaks at 284.6, 286.2, 287, and 288.5 eV that are assigned to graphitic, C≡N, amide-type, and carboxylic-type carbon, respectively [32]. Thus, the chemical nature of Se as SeCN is confirmed by the C≡N signature in both the C 1s and N 1s spectra.

The topographical and morphological HRTEM analysis revealed that CD-SeCN is spherical nanoparticles with an average diameter of 2.5 ± 0.68 nm, the coefficient of variance being 0.27 (Fig. 3). As expected from the carbonaceous core, the UV–vis absorption spectrum presents a shoulder at 325 nm, ascribed to the presence of the C=O bond and their n–π* transitions, which might be influenced by the surface groups [33]. CD-SeCN exhibits the typical photoluminescence properties of CDs, with an emission spectrum peaking at 450 nm (Fig. 3) and a quantum yield of 2%. Remarkably, treatment with H_2O_2 had no effect on the fluorescence of CD-SeCN (Fig. 4(a)). This observation is in contrast with the behavior of SeCDs, whose fluorescence has been reported to depend on the oxidation state of Se, which increases upon incubation with H_2O_2 and reverses after reduction with GSH [20, 21]. This negative result can be rationalized when considering that the enhancement of the fluorescence of SeCDs is attributed to the oxidation of Se to seleninic acid [21], a transformation that SeCN does not undergo at low concentrations of H_2O_2 and room temperature [34]. However, after incubation with 2-mercaptoethanol, a remarkable unexpected improvement in intensity was observed (Fig. 4(b)), though the effect decayed with time in a linearly dependent manner (Fig. 4(c)), indicating that the surface modification is not limited to the transformation of SeCN into selenyl sulfide [35].

3.2 GPx-like activity of CD-SeCN

GPxs protect cells from oxidative damage. Since the discovery that ebselen mimics the catalytic activity of GPxs and the influence of the atoms/interactions around the Se atom, the GPx-like activity of Se-bearing systems has attracted major interest [36, 37]. For the particular case of the SeCN functional group, the link between this chemical form of Se and the GPx-like activity is known from the first studies on diets supplemented with benzylselenocyanate [38]. More recently, a weak GPx-like activity has been reported in some molecules containing the SeCN function, although most of them were inactive [29]. However, the environment of the Se in CD-SeCN is peculiar since the SeCN group is attached to the carbonaceous core by an amide bond spanned by a three carbon chain and in close proximity to a carboxylate group (Scheme 1). These features may influence the GPx-like activity of the SeCN group. Additionally, to the best of our knowledge, SeCDs have not been reported as GPx mimics. These facts encouraged us to study the GPx-like activity of CD-SeCN.

AA-CD did not show GPx-like activity. Providing that Se is responsible for GPx-like activity and the XPS analysis led to an estimate of the content of Se as 0.36 μmol per milligram of CD-SeCN, the study was conducted in terms of the concentration of Se atoms instead of the concentration of nanoparticles, allowing the comparison with ebselen. Given the insolubility of ebselen in water, the ability to reduce H_2O_2 (2 mM) using thiophenol (1 mM) as a reductant was evaluated in methanol, as described by Iwaoka and Tomada [24]. The results of the relationship between the GPx-like activity and content in Se show that, within the experimental conditions and the range of concentrations assayed, ebselen and KSeCN show a poor performance regardless of the concentration of Se, whereas CD-SeCN mimics GPx, with a clear linear relationship between the content in Se and the catalytic activity (Fig. 5).

Coined by Scrimin and coworkers in 2004, the term nanozyme has been recently used to refer to gold nanoparticles functionalized with a peptide containing selenocysteine that catalyzes the

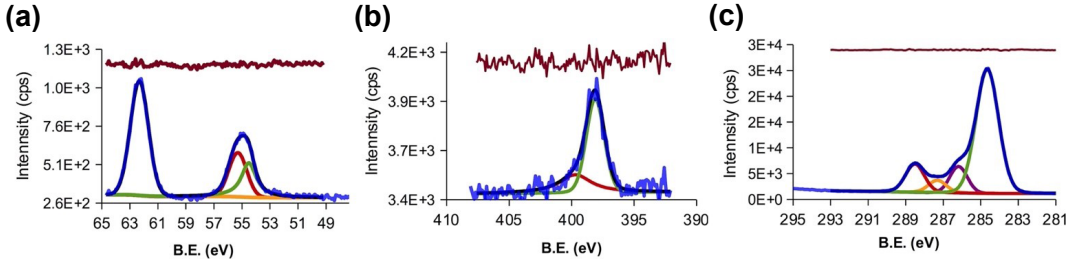

Figure 2 (a) Se 3d, (b) N 1s, and (c) C 1s high resolution XPS spectra of CD-SeCN.

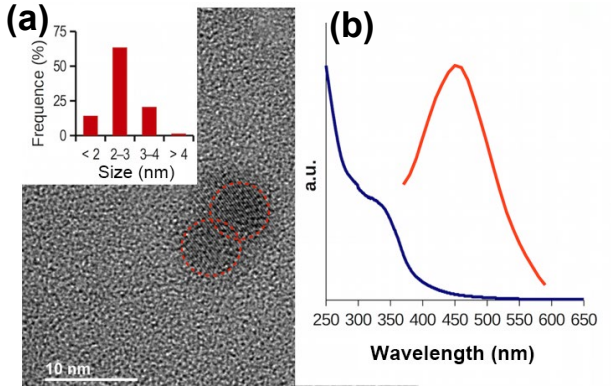

Figure 3 (a) HRTEM image of two large CD-SeCN nanoparticles (insert shows size distribution). (b) UV–vis absorption (blue) and photoluminescence emission (red) spectra of CD-SeCN (excitation at 308 nm).

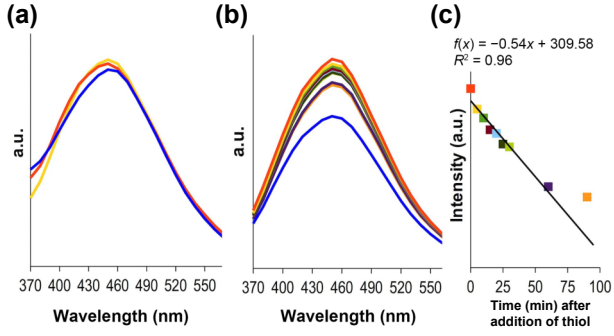

Figure 4 Photoluminiscence of CD-SeCN (blue) upon the addition of 5 μL of either (a) H_2O_2 (49 mM) or (b) 2-mercaptoethanol (45 mM), and (c) linear decay with time of the increase in intensity upon addition of 2-mercaptoethanol.

reduction of H_2O_2 by GSH [39]. Given the similarity with CD-SeCN (i.e., a nanoparticle as a nanoplatform with Se-bearing appendants as active sites), the reaction was evaluated. Considering a blood volume of 5 L and that doses of Se beyond 400 μg/day (i.e., 5.1 μmol/day) are pro-oxidant [40], a concentration of 5 μg/mL of CD-SeCN (i.e., 1.8 μM of Se) was assayed at physiological (7.0) and tumoral (6.5) pH values, and concentrations of GSH in the millimolar physiological range up to 5 mM. As depicted in Fig. 6(a), there exists a linear relationship between the catalytic activity and the concentration of GSH at pH 7. However, the trend is different at pH 6.5, and the activity is higher at low concentrations of GSH up to 3 mM and then declines. These results support the GPx-like activity of CD-SeCN under physiological conditions and suggest a limited antioxidant activity in tumoral cells.

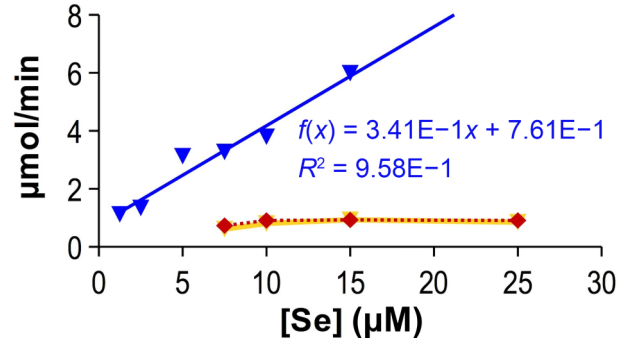

Figure 5 GPx-like activity of Se from CD-SeCN (blue), KSeCN (yellow), and ebselen (red) to reduce H_2O_2 (2 mM) using thiophenol (1 mM) as reductant in methanol.

The facts that the incubation of CD-SeCN with GSH enhances the fluorescence and that it is well established that arylthiols transform SeCN into selenyl sulfide [35] led us to hypothesize that selenyl sulfide is the chemical species responsible for the GPx-like activity. However, the revised mechanism of ebselen suggests a diselenide intermediate formed from the selenyl sulfide by disproportionation, the rate limiting step of the overall catalytic reaction being the transformation of selenyl sulfide into diselenide [41]. To gain insight into the GPx-like activity of CD-SeCN, the reaction was further studied by ^{77}SeNMR. Different attempts to obtain good ^{77}SeNMR spectra of CD-SeCN failed, and this complication was not unexpected given the difficulties often found when using NMR with nanoparticles [42]. The challenge was then approached by neglecting the effect of the carbonaceous core and assuming that the catalytic activity relies on the SeCN moiety to conclude that compound **1** is a suitable model system. As shown in Fig. 6(b), the ^{77}SeNMR spectrum of compound **1** shows a single signal at 216 ppm that corresponds to SeCN. After the addition of 5 equivalents of 2-mercaptoethanol (i.e., the simplest hydrosoluble thiol), the signal shifted downfield to 372 ppm and during the catalysis, this was the only species detected (Fig. S2 in the ESM). This chemical shift is compatible with a diselenide function and to assess the identification of its chemical nature, the expected diselenide from compound **1** (i.e., compound **2**) was synthesized. However, the ^{77}SeNMR spectrum of compound **2** showed a single signal at 290 ppm (Fig. S3 in the ESM), discarding the initial assignment to a diselenide and suggesting that it corresponds to the selenyl sulfide. These results do not rule out the formation of a diselenide form during the catalytic cycle since its life may be too short to be detected, the signal being disguised as the baseline, in full agreement with the revised mechanism of ebselen that identifies the disproportionation reaction of selenyl sulfide as the

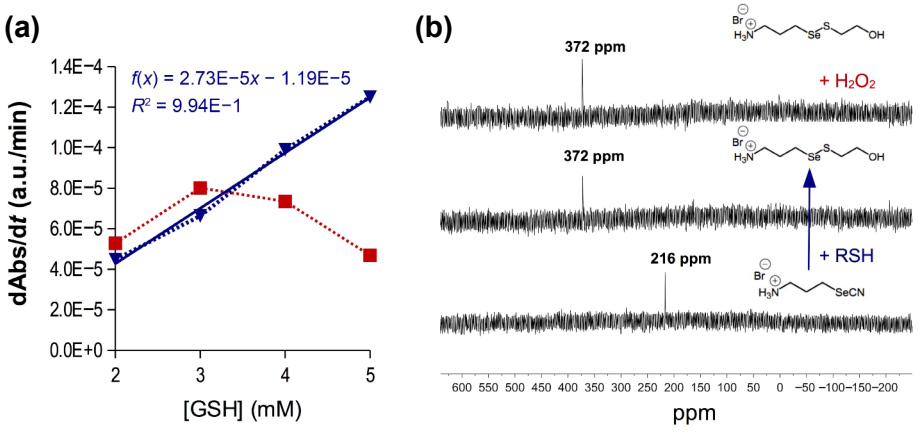

Figure 6 (a) GPx-like activity of CD-SeCN (5 μg/mL) against H_2O_2 (2 mM) as a function of the concentration of glutathione at pH 7.0 (blue) and pH 6.5 (red). For each point, the correlation coefficient of the linear fitting was higher than 0.9. The linear fit of the data at pH 7 is shown. (b) ^{77}SeNMR of compound **1** in D_2O (bottom), after the addition of 5 equivalents of 2-mercaptoethanol (center), and during the catalysis of 10 equivalents of H_2O_2 (top).

limiting step in the overall catalytic reaction [41]. The results of the enhancement of the fluorescence of CD-SeCN in the presence of 2-mercaptoethanol followed by a slow decline with time (Fig. 4(c)) point to the transformation of the expected selenyl sulfide species into a different species that may be the diselenide form.

3.3 Assay of CD-SeCN on cell cultures

SeNPs are attracting major interest in biomedicine and have been identified as promising therapeutic agents in cancer [12, 13, 40]. Furthermore, organoselenium compounds have thiol-oxidizing properties, and studies with 1,4-phenylenebis(methylene) selenocyanate in prostate cancer found a decrease in GSH levels, implying an increase in intracellular oxidative stress or a change in the GSH/glutathione disulfide (GSSG) ratio [5, 28]. Indeed, changes in the GSH antioxidant system have been implicated in tumor initiation, progression, and response to treatment and it is targeted by some novel therapies [43]. With this background, we hypothesized that CD-SeCN may have pharmacological applications. To assess our hypothesis, the biological effect of CD-SeCN was evaluated against the cell lines HEK293 and A549 that produce different levels of GSH per milligram of protein, being 65.6 ± 12 nmol for HEK293 and 106.0 ± 11.0 nmol for A549 [44].

We have previously reported that CDs obtained from the thermolysis of citric acid are not toxic to different cell lines up to 250 μg/mL, even when the surface is modified, and that HEK293 cells show good tolerance up to 200 μg/mL (i.e., a survival rate higher than 80%) of amphiphilic-like CDs obtained by amidation of AA-CD with alkyl amines [23, 26]. On this basis, the toxicity of CD-SeCN was assayed up to 250 μg/mL on both HEK293 and A549 cells at 24 and 48 h. Cells were analyzed by flow cytometry after staining with FDA and PI (Fig. S4 in the ESM). Data at 24 h revealed that concentrations of CD-SeCN as low as 10 μg/mL yield a survival rate lower than 50%, regardless of the cell line although HEK293 cells that produce lower basal level of GSH are less resistant than A549 cells. The scene is completely different at 48 h with a survival rate close to 70% for 10 μg/mL and higher than 25% for concentrations beyond 200 μg/mL. These findings show that functionalizing the surface of CDs with SeCN produces nanoparticles whose toxicity depends on the intracellular level of GSH in the short term, but that over time, the surviving cells grow as if the concentration of CD-SeCN were much lower. To contextualize these results of cytotoxicity, it is important to recall that the content of Se in CD-SeCN is 0.36 μmol per milligram of nanoparticle and that for a blood volume of 5 liters, the concentrations assayed imply the administration of a dose that ranges from 1.4 to 35.9 mg of Se, which are far beyond the 0.4 mg/day tolerated by adults [40].

A narrower concentration range up to 10 μg/mL, equivalent to 3.6 times the dose tolerated by adults, was assayed, and membrane changes indicative of apoptosis or necrosis of the cells were evaluated. Data on cell viability confirmed the results of the previous experiment, and, as expected, cell viability was found to depend on both dose and time. At 24 h the viability is influenced by the intracellular GSH concentration, with A549 almost unaffected, whereas the viability of HEK293, with half content of GSH, was compromised even at a concentration of CD-SeCN that yields an amount of Se equivalent to 0.9 times the dose tolerated by adults (Fig. 7(a)). The toxicity of CD-SeCN vanished at 48 h (Fig. 7(c)). The results at 24 h are in full agreement with studies that have demonstrated that the apoptotic effect of Se in GSH deprived cells increases concomitantly with the decrease in GSH levels [45]. However, results at 48 h are counterintuitive, especially when considering the toxicity of different metal ions, which increases with time and dose [46, 47], and strongly suggest that CD-SeCN nanoparticles are consumed or deactivated by the cells. This deactivation is not entirely unexpected since the degradation of carbon-based nanomaterials by peroxidase enzymes is well established [48], and it highlights the carbonaceous nature of CD-SeCN.

The process that results in cell death is an important parameter because, whereas apoptosis results in the clearance of the cell with minimal damage to the surrounding tissues, necrosis results in the uncontrolled death of the cell, which undergoes cytolysis and induces an inflammatory response in the affected tissue. Membrane changes indicative of apoptosis or necrosis of the cells were evaluated by determining the uptake of annexin V-FITC/PI double staining. Cells suffering apoptosis bind annexin V, at the late stage also PI, while necrotic cells bind only PI (Figs. S5 and S6 in the ESM). To study the prevalence of necrosis or apoptosis the ratio of necrotic/apoptotic cells was calculated, with ratios > 1 revealing the prevalence of necrosis. Results show that cell death proceeds via apoptosis in the absence of CD-SeCN (control cells), and in A549 cells regardless of the concentration of CD-SeCN or the time of incubation, confirming their invulnerability (Figs. 7(b) and 7(d)). However, HEK293 cells die by necrosis at 24 h, although the ratio of 1.6 suggests a moderate extent, and at 48 h by apoptosis, as the cells do in the absence of CD-SeCN, further supports the biosafety of CD-SeCN and their pharmacological potential, particularly in those pathologies such as brain tumors and some gastrointestinal cancers (esophagus, stomach, and liver) that present lower GSH levels compared to disease-free tissues [49].

4 Conclusions

To summarize, the reaction of AA-CD used as a nanoplatform with Se-bearing amines is a straightforward general strategy to append chemically defined Se and other chalcogens on the surface of CDs. As a proof of concept, we have obtained CDs decorated with SeCN motifs.

The SeCN functionalization transforms the inert CDs into nanoparticles with biological properties. CD-SeCN shows *in vitro* GPx-like activity, and, compared to ebselen and KSeCN, CD-SeCN is more active. When evaluated at physiological (7.0) and tumoral (6.5) pH values with the physiological reductant GSH,

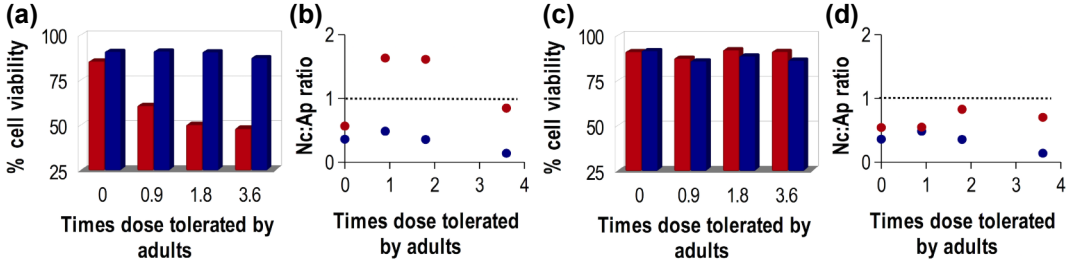

Figure 7 Viability of HEK293 (red) and A549 (blue) cells incubated with different concentrations of CD-SeCN to yield different numbers of doses tolerated by adults for (a) 24 h and (c) 48 h, and ((b) and (d)) corresponding necrosis/apoptosis ratios. Ratios below 1 indicate that apoptosis prevails over necrosis as the process that leads to cell death.

results indicate a different behavior in tumoral cells. Additionally, the SeCN moiety turns the highly biocompatible CDs into cytotoxic nanoparticles especially effective toward cells whose levels of GSH are low, inducing necrosis. Interestingly, toxicity is limited in time, and at 48 h the cell growth is almost recovered and the mechanism of cell death switches back to apoptosis. These results support a future evaluation of CD-SeCN as therapeutic nanoparticles.

In addition to making Se-containing nanosystems with this Janus behavior, where one side is an antioxidant and the other is a pro-oxidant, our method shows that using AA-CD as nanoplatforms is easy and flexible. This opens the door to making more complex nanosystems that, in addition to the biological properties of Se, can carry other molecules that give the nanoparticles more functions.

Given the prospective applications of CD nanomaterials and the biological applications of SeNP, the authors foresee future clinical applications of CD nanomaterials functionalized with Se-containing functional groups. To assess the full potential of these unique materials, substantial additional research is required to better understand the mechanisms underlying the biophysiological effects of Se.

Acknowledgements

This work was financially supported by the Spanish institution Ministerio de Ciencia, Innovacion y Universidades (No. CTQ2017-86125-P). We would like to thank Unit of Excellence in Chemistry Applied to Biomedicine and the Environment and Jaime Lazuen (flow cytometry), Nieves Rodriguez (cell culture), and Laura Mendez (XPS Facility) from Centro de Instrumentación Científica (Universidad de Granada) for their support.

Funding note: Open Access funding provided thanks to the Universidad de Granada/CBUA agreement with Springer Nature.

Electronic Supplementary Material: Supplementary material (^{77}SeNMR of compound **2** and flow cytometry studies of cytotoxicity and cell death mechanism) is available in the online version of this article at https://doi.org/10.1007/s12274-023-5442-3.

References

[1] Rotruck, J. T.; Pope, A. L.; Ganther, H. E.; Swanson, A. B.; Hafeman, D. G.; Hoekstra, W. G. Selenium: Biochemical role as a component of glutathione peroxidase. *Science* **1973**, *179*, 588–590.

[2] Reich, H. J.; Hondal, R. J. Why nature chose selenium. *ACS Chem. Biol.* **2016**, *11*, 821–841.

[3] Sies, H.; Jones, D. P. Reactive oxygen species (ROS) as pleiotropic physiological signalling agents. *Nat. Rev. Mol. Cell Biol.* **2020**, *21*, 363–383.

[4] Hayes, J. D.; Dinkova-Kostova, A. T.; Tew, K. D. Oxidative stress in cancer. *Cancer Cell* **2020**, *38*, 167–197.

[5] Nogueira, C. W.; Barbosa, N. V.; Rocha, J. B. T. Toxicology and pharmacology of synthetic organoselenium compounds: An update. *Arch. Toxicol.* **2021**, *95*, 1179–1226.

[6] Wang, J.; Wang, P.; Dong, C. J.; Zhao, Y.; Zhou, J. X.; Yuan, C. L.; Zou, L. L. Mechanisms of ebselen as a therapeutic and its pharmacology applications. *Future Med. Chem.* **2020**, *12*, 2141–2160.

[7] Kunwar, A.; Priyadarsini, K. I. History and development of selenium-based radioprotectors: Distinctions between the inorganic and organic forms. In *Organoselenium Compounds in Biology and Medicine*: *Synthesis*, *Biological and Therapeutic Treatments*. Jain, V. K.; Priyadarsini, K. I., Eds.; Royal Society of Chemistry: Cambridge, 2017; pp 317–341.

[8] Rocha, J. B. T.; Oliveira, C. S.; Nogara, P. A. Toxicology and anticancer activity of synthetic organoselenium compounds. In *Organoselenium Compounds in Biology and Medicine*: *Synthesis*, *Biological and Therapeutic Treatments*. Jain, V. K.; Priyadarsini, K. I., Eds.; Royal Society of Chemistry: Cambridge, 2017; pp 342–376.

[9] Fernandes, A. P.; Gandin, V. Selenium compounds as therapeutic agents in cancer. *Biochim. Biophys. Acta (BBA)-Gen. Subj.* **2015**, *1850*, 1642–1660.

[10] Bisht, N.; Phalswal, P.; Khanna, P. K. Selenium nanoparticles: A review on synthesis and biomedical applications. *Mater. Adv.* **2022**, *3*, 1415–1431.

[11] Ali, W.; Álvarez-Pérez, M.; Marć, M. A.; Salardón-Jiménez, N.; Handzlik, J.; Domínguez-Álvarez, E. The anticancer and chemopreventive activity of selenocyanate-containing compounds. *Curr. Pharmacol. Rep.* **2018**, *4*, 468–481.

[12] Khurana, A.; Tekula, S.; Saifi, M. A.; Venkatesh, P.; Godugu, C. Therapeutic applications of selenium nanoparticles. *Biomed. Pharcother.* **2019**, *111*, 802–812.

[13] Nayak, V.; Singh, K. R. B.; Singh, A. K.; Singh, R. P. Potentialities of selenium nanoparticles in biomedical science. *New J. Chem.* **2021**, *45*, 2849–2878.

[14] Manjunatha, C.; Rao, P. P.; Bhardwaj, P.; Raju, H.; Ranganath, D. New insight into the synthesis, morphological architectures and biomedical applications of elemental selenium nanostructures. *Biomed. Mater.* **2021**, *16*, 022010.

[15] Zambonino, M. C.; Quizhpe, E. M.; Jaramillo, F. E.; Rahman, A.; Santiago Vispo, N.; Jeffryes, C.; Dahoumane, S. A. Green synthesis of selenium and tellurium nanoparticles: Current trends, biological properties and biomedical applications. *Int. J. Mol. Sci.* **2021**, *22*, 989.

[16] Yi, C. X.; Yu, Z. H.; Sun, X.; Zheng, X.; Yang, S. Y.; Liu, H. C.; Song, Y.; Huang, X. FA/Mel@ZnO nanoparticles as drug self-delivery systems for RPE protection against oxidative stress. *Adv. Nano Res.* **2022**, *13*, 87–96.

[17] Truskewycz, A.; Yin, H.; Halberg, N.; Lai, D. T. H.; Ball, A. S.; Truong, V. K.; Rybicka, A. M.; Cole, I. Carbon dot therapeutic platforms: Administration, distribution, metabolism, excretion, toxicity, and therapeutic potential. *Small* **2022**, *18*, 2106342.

[18] Bayda, S.; Amadio, E.; Cailotto, S.; Frión-Herrera, Y.; Perosa, A.; Rizzolio, F. Carbon dots for cancer nanomedicine: A bright future. *Nanoscale Adv.* **2021**, *3*, 5183–5221.

[19] Miao, S. H.; Liang, K.; Zhu, J. J.; Yang, B.; Zhao, D. Y.; Kong, B. Hetero-atom-doped carbon dots: Doping strategies, properties and applications. *Nano Today* **2020**, *33*, 100879.

[20] Zhou, D. L.; Huang, H.; Yu, J. R.; Hu, Z. M. Lysosome-targetable selenium-doped carbon nanodots for *in situ* scavenging free radicals in living cells and mice. *Microchim. Acta* **2021**, *188*, 223.

[21] Li, F.; Li, T. Y.; Sun, C. X.; Xia, J. H.; Jiao, Y.; Xu, H. P. Selenium-doped carbon quantum dots for free-radical scavenging. *Angew. Chem., Int. Ed.* **2017**, *56*, 9910–9914.

[22] Zhang, L.; Sun, C. X.; Tan, Y. Z.; Xu, H. P. Selenium-sulfur-doped carbon dots with thioredoxin reductase activity. *CCS Chem.* **2021**, *4*, 2239–2248.

[23] Ortega-Muñoz, M.; Vargas-Navarro, P.; Hernandez-Mateo, F.;

Salinas-Castillo, A.; Capitan-Vallvey, L. F.; Plesselova, S.; Salto-Gonzalez, R.; Giron-Gonzalez, M. D.; Lopez-Jaramillo, F. J.; Santoyo-Gonzalez, F. Acid anhydride coated carbon nanodots: Activated platforms for engineering clicked (bio)nanoconstructs. *Nanoscale* **2019**, *11*, 7850–7856.

[24] Iwaoka, M.; Tomoda, S. A model study on the effect of an amino group on the antioxidant activity of glutathione peroxidase. *J. Am. Chem. Soc.* **1994**, *116*, 2557–2561.

[25] Würth, C.; Grabolle, M.; Pauli, J.; Spieles, M.; Resch-Genger, U. Relative and absolute determination of fluorescence quantum yields of transparent samples. *Nat. Protoc.* **2013**, *8*, 1535–1550.

[26] Ortega-Muñoz, M.; Vargas-Navarro, P.; Plesselova, S.; Giron-Gonzalez, M. D.; Iglesias, G. R.; Salto-Gonzalez, R.; Hernandez-Mateo, F.; Delgado, A. V.; Lopez-Jaramillo, F. J.; Santoyo-Gonzalez, F. Amphiphilic-like carbon dots as antitumoral drug vehicles and phototherapeutical agents. *Mater. Chem. Front.* **2021**, *5*, 8151–8160.

[27] El-Bayoumy, K. Effects of organoselenium compounds on induction of mouse forestomach tumors by benzo(a)pyrene. *Cancer Res.* **1985**, *45*, 3631–3635.

[28] Pinto, J. T.; Sinha, R.; Papp, K.; Facompre, N. D.; Desai, D.; El-Bayoumy, K. Differential effects of naturally occurring and synthetic organoselenium compounds on biomarkers in androgen responsive and androgen independent human prostate carcinoma cells. *Int. J. Cancer* **2007**, *120*, 1410–1417.

[29] Nie, Y. S.; Zhong, M.; Li, S. L.; Li, X. L.; Zhang, Y. M.; Zhang, Y. H.; He, X. R. Synthesis and potential anticancer activity of some novel selenocyanates and diselenides. *Chem. Biodivers.* **2020**, *17*, e1900603.

[30] He, X. R.; Zhong, M.; Li, S. L.; Li, X. L.; Li, Y. Y.; Li, Z. T.; Gao, Y. G.; Ding, F.; Wen, D.; Lei, Y. C. et al. Synthesis and biological evaluation of organoselenium (NSAIDs-SeCN and $SeCF_3$) derivatives as potential anticancer agents. *Eur. J. Med. Chem.* **2020**, *208*, 112864.

[31] Biesinger, M. C. X-ray Photoelectron Spectroscopy (XPS) Reference Pages [Online]. http://www.xpsfitting.com/ (accessed Nov 17, 2021).

[32] Graf, N.; Yegen, E.; Gross, T.; Lippitz, A.; Weigel, W.; Krakert, S.; Terfort, A.; Unger, W. E. S. XPS and NEXAFS studies of aliphatic and aromatic amine species on functionalized surfaces. *Surf. Sci.* **2009**, *603*, 2849–2860.

[33] Hola, K.; Zhang, Y.; Wang, Y.; Giannelis, E. P.; Zboril, R.; Rogach, A. L. Carbon dots—Emerging light emitters for bioimaging, cancer therapy and optoelectronics. *Nano Today* **2014**, *9*, 590–603.

[34] Ganther, H. E. Selenotyrosine and related phenylalanine derivatives. *Bioorgan. Med. Chem.* **2001**, *9*, 1459–1466.

[35] Clark, E. R.; Al-Turaihi, M. A. S. The reaction of *o*-nitro- and *p*-nitro-phenyl selenocyanates with arylthiols. *J. Organomet. Chem.* **1977**, *134*, 181–187.

[36] Bhabak, K. P.; Mugesh, G. Functional mimics of glutathione peroxidase: Bioinspired synthetic antioxidants. *Acc. Chem. Res.* **2010**, *43*, 1408–1419.

[37] Mukherjee, A. J.; Zade, S. S.; Singh, H. B.; Sunoj, R. B. Organoselenium chemistry: Role of intramolecular interactions. *Chem. Rev.* **2010**, *110*, 4357–4416.

[38] Reddy, B. S.; Sugie, S.; Maruyama, H.; El-Bayoumy, K.; Marra, P. Chemoprevention of colon carcinogenesis by dietary organoselenium, benzylselenocyanate, in F344 rats. *Cancer Res.* **1987**, *47*, 5901–5904.

[39] Zhang, D. C.; Shen, N.; Zhang, J. R.; Zhu, J. M.; Guo, Y.; Xu, L. A novel nanozyme based on selenopeptide-modified gold nanoparticles with a tunable glutathione peroxidase activity. *RSC Adv.* **2020**, *10*, 8685–8691.

[40] Ferro, C.; Florindo, H. F.; Santos, H. A. Selenium nanoparticles for biomedical applications: From development and characterization to therapeutics. *Adv. Healthc. Mater.* **2021**, *10*, 2100598.

[41] Bhowmick, D.; Mugesh, G. Insights into the catalytic mechanism of synthetic glutathione peroxidase mimetics. *Org. Biomol. Chem.* **2015**, *13*, 10262–10272.

[42] Mayer, C. NMR studies of nanoparticles. *Annu. Rep. NMR Spectrosc.* **2005**, *55*, 205–258.

[43] Kennedy, L.; Sandhu, J. K.; Harper, M.-E.; Cuperlovic-Culf, M. Role of glutathione in cancer: From mechanisms to therapies. *Biomolecules* **2020**, *10*, 1429.

[44] Giustarini, D.; Galvagni, F.; Tesei, A.; Farolfi, A.; Zanoni, M.; Pignatta, S.; Milzani, A.; Marone, I. M.; Dalle-Donne, I.; Nassini, R. et al. Glutathione, glutathione disulfide, and *S*-glutathionylated proteins in cell cultures. *Free Radic. Biol. Med.* **2015**, *89*, 972–981.

[45] Ranawat, P.; Bansal, M. P. Decreased glutathione levels potentiate the apoptotic efficacy of selenium: Possible involvement of p38 and JNK MAPKs—*In vitro* studies. *Mol. Cell Biochem.* **2008**, *309*, 21–32.

[46] Granchi, D.; Cenni, E.; Ciapetti, G.; Savarino, L.; Stea, S.; Gamberini, S.; Gori, A.; Pizzoferrato, A. Cell death induced by metal ions: Necrosis or apoptosis? *J. Mater. Sci. -Mater. Med.* **1998**, *9*, 31–37.

[47] Catelas, I.; Petit, A.; Vali, H.; Fragiskatos, C.; Meilleur, R.; Zukor, D. J.; Antoniou, J.; Huk, O. L. Quantitative analysis of macrophage apoptosis vs. necrosis induced by cobalt and chromium ions *in vitro*. *Biomaterials* **2005**, *26*, 2441–2453.

[48] Mokhtari-Farsani, A.; Hasany, M.; Lynch, I.; Mehrali, M. Biodegradation of carbon-based nanomaterials: The importance of "biomolecular corona" consideration. *Adv. Funct. Mater.* **2022**, *32*, 2105649.

[49] Gamcsik, M. P.; Kasibhatla, M. S.; Teeter, S. D.; Colvin, O. M. Glutathione levels in human tumors. *Biomarkers* **2012**, *17*, 671–691.